THE JOURNAL OF PHYSICAL CHEMISTRY C

Article

pubs.acs.org/JPCC

Understanding Thermal Quenching of Photoluminescence in Oxynitride Phosphors from First Principles

Samuel Poncé,*[,†,‡] Yongchao Jia,[†,‡] Matteo Giantomassi,[†,‡] Masayoshi Mikami,[¶] and Xavier Gonze[†,‡]

[†]Institute of Condensed Matter and Nanosciences, Université catholique de Louvain, Chemin des étoiles 8, bte L07.03.01, B-1348 Louvain-la-neuve, Belgium

[‡]European Theoretical Spectroscopy Facility

[¶]MCHC R&D Synergy Center, Inc. 1000, Kamoshida-cho Aoba-ku, Yokohama, 227-8502, Japan

ABSTRACT: Understanding the physical mechanisms behind thermal effects in phosphors is crucial for white light-emitting device (WLEDs) applications, as thermal quenching of their photoluminescence might render them useless. We analyze from first-principles, before and after absorption/emission of light, two chemically close Eu-doped $Ba_3Si_6O_{12}N_2$ and $Ba_3Si_6O_9N_4$ crystals for WLEDs. The first one has an almost constant emission intensity with increasing temperature whereas the other one does not. Our results, in which the Eu-5d levels are obtained inside the band gap thanks to the removal of an electron from the $4f^7$ shell, and the atomic neighborhood properly relaxed in the excited state, attributes the above-mentioned experimental difference to an autoionization model of the thermal quenching, based on the energy difference between Eu_{5d} and the conduction band minimum. Our *depleted-shifted 4f* method can identify luminescent centers and therefore allows for effective crystal site engineering of luminescent centers in phosphors from first principles.

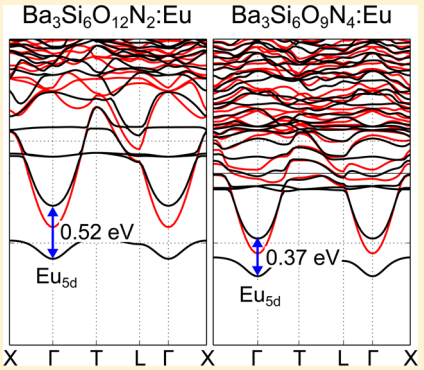

1. INTRODUCTION

White light-emitting devices (WLEDs) that combine III-nitride-based electroluminescent diodes and rare-earth (RE) doped photoluminescent materials are seen as one of the most promising light source to replace incandescent and ultraviolet (UV) lamps. The current major challenge faced by WLEDs is the tailoring of photoluminescence spectra[1] to achieve the desired color rendering index with high thermal stability.[2] Such tailoring is usually achieved by crystal site engineering and good understanding of the phosphor electronic band structures.

The phosphor-converted WLEDs rely on multiple layers of rare-earth (RE) doped photoluminescent materials called "phosphors" to down-convert (Stokes shift) the monochromatic UV or blue light from an electroluminescent diode into a broad-spectrum white light. The photoluminescent properties in RE-doped phosphors are most often based on radiative 5d-4f transition of the dopant.

A phenomenological model of the luminescence and of the Stokes shift of such phosphors is based on configurational diagrams[3,4] (see Figure 1). In the case of RE-doped phosphors, one electron is excited from the RE-4f band into the excited RE-5d band by a UV/blue photon coming from the diode (absorption). Such excited RE-5d electron modifies the forces inside the material, changing the average atomic positions from X_0 to X_0^*. After dissipation of the energy as phonons, the excited electron spontaneously emits light and the crystal returns to its original ground-state geometry after yet another relaxation.

Unfortunately for the WLEDs industry, other nonradiative mechanisms allow the RE-5d electron to relax to the ground

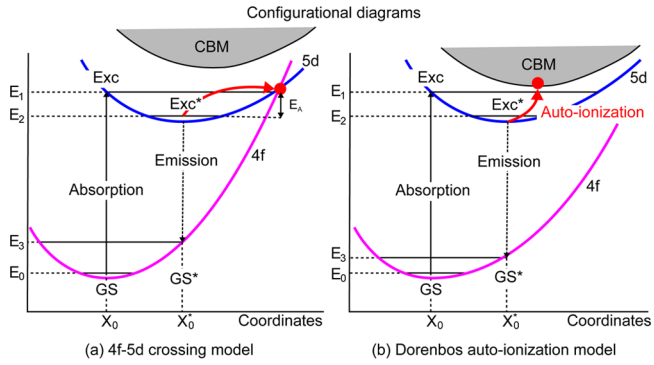

Figure 1. Comparison between the 4f−5d crossing and the Dorenbos autoionization models to explain the thermal quenching.

state. For example, the electron can lose entirely its energy as heat by emitting phonons or transfer its energy to impurities or defects called "killer-center" via, for example, photoionization.[5] A phosphor can have high photoluminescence efficiency at low temperature but little at working temperature. The existence of such thermal quenching seems to be sensitive to minute details of the host material and RE dopants.

A striking example is given by two chemically close oxynitride materials: $Ba_3Si_6O_{12}N_2$:Eu and $Ba_3Si_6O_9N_4$:Eu (named generically BSON compounds). The two hosts

Received: December 17, 2015
Revised: February 3, 2016
Published: February 5, 2016

DOI: 10.1021/acs.jpcc.5b12361
J. Phys. Chem. C 2016, 120, 4040−4047

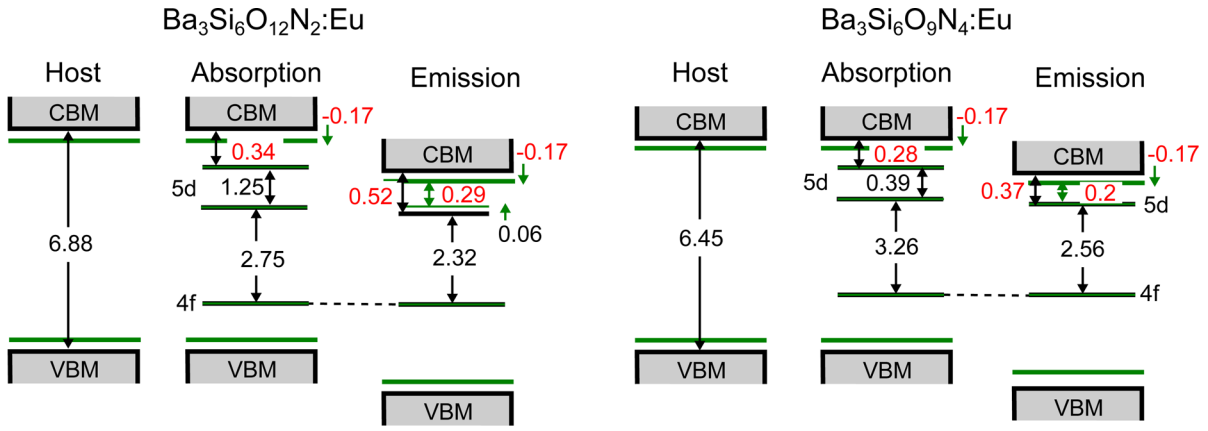

Figure 2. Absorption and emission levels (eV) of the two BSON luminescent centers from experimental data or G_0W_0 calculations (in black) and present calculations (in red). The horizontal band positions at 0 K are shown in black, and at 300 K are shown in green (sometimes superimposed when there is no thermal effect). The −0.17 eV temperature effect is the sum of the zero-point motion effect −0.12 eV and temperature dependence (see Figure 5). The absorption and emission energy differences are relative to the ground state of the doped system, with the 4f level being taken as zero-energy reference (see text for details).

materials have very similar electronic and structural properties[6] but when doped with Eu, they exhibit different luminescence characteristics and associated temperature behavior. The green phosphor $Ba_3Si_6O_{12}N_2$:Eu[7−17] has an intensity that stays almost constant with temperature up to its working temperature, while $Ba_3Si_6O_9N_4$:Eu is a bluish-green phosphor[8,18−21] that exhibits an unfavorable decrease of the luminescence intensity with temperature.

The experimental absorption and emission spectra as well as their temperature dependence have been measured experimentally[7] and lead to a full width at half-maximum (fwhm) of the two emission curves at 4 K of 1500 and 1300 cm^{-1} for $Ba_3Si_6O_{12}N_2$:Eu and $Ba_3Si_6O_9N_4$:Eu, respectively. These two FWHMs are considered rather narrow and therefore it is expected that the luminescence in both compounds only comes from one luminescent center for each material (one nonequivalent crystallographic position), despite the existence of several Ba inequivalent sites (two in $Ba_3Si_6O_{12}N_2$ and three in $Ba_3Si_6O_9N_4$), where substitution by Eu may occur.

In this paper, we clarify the physical origin of the thermal quenching in these RE-doped oxynitrides, by complementing the available experimental data with first-principle results. Additionally, we confirm the uniqueness of the nonequivalent luminescent site that is present in both doped materials, which can explain the origin of rather narrow fwhm in both BSON compounds. We believe that our developed method may be effective not only for identification but also for the design of luminescent centers in other RE-doped phosphors.

Because of the size of the cells needed to represent the doped materials, the Bethe−Salpeter equation (BSE),[22] presently the best technique to predict optical properties in solids, could not be straightforwardly used. We rely instead on a simpler mean-field approach, in which a fixed 4f hole is introduced, either frozen in the core by means of a pseudopotential, or artificially forced inside the band gap so that the Eu_{5d} state is located inside the band gap. This approach allows us to draw, for the first time, a global and coherent picture of the absorption/emission, the geometry relaxation and the temperature effect on the luminescence.

In this paper, we first present two competing models to describe thermal quenching (section 2) and use density-functional theory(DFT)-based level of theory to describe ground-state (section 3) and excited-states (section 4) properties in order to validate Dorenbos autoionization model. The quantitative assessment of the RE-5d to conduction band minimum (CBM) gaps requires some care to avoid self-interaction of the excited electron that is discussed in section 5. Finally, we present in section 6 additional tests to strengthen our proposed *depleted-shifted 4f* approach.

2. MODELS FOR THE THERMAL QUENCHING

Most models for the thermal quenching rely on a configurational diagram that shows energy versus ionic degrees of freedom for the ground-state as well as the excited-state of a material. Such configurational diagrams are extremely successful at explaining luminescence processes and Stokes shifts. However, different mechanisms can explain thermal quenching. The 5d-4f crossing decay model (Figure 1a) predicts that large atomic geometry changes lead to the crossing of the Eu_{5d} and Eu_{4f} configurational energy curves. If the temperature is large enough, the excited electron of the 5d band overcomes the activation energy barrier E_A and decays nonradiatively to the ground state. Such decay model has been shown by Mikami and co-worker[8,23,24] to contradict the observed thermal quenching.

In contrast, Dorenbos[25] proposed an autoionization model, see Figure 1b, arguing that the Eu_{5d} comes close to the conduction band minimum (CBM) from the host material well before the 5d−4f crossing point. We will show later that indeed this situation can be inferred from first-principles calculations. At working temperature, the Eu_{5d} electron is transferred to the conduction band, becomes delocalized and mobile, and undergoes energy dissipation through other nonradiative mechanisms (trapping, killer centers such as defects, lattice vibration···). On the basis of this model, the smaller the Eu_{5d}-CBM gap, the larger is the thermal quenching. Dorenbos' empirical formula[25] CBM-Eu_{5d} = $\frac{T_{0.5}}{680}$ eV links the size of this gap to the quenching temperature $T_{0.5}$, at which the emission intensity has dropped by 50% from its low temperature value. From experimental thermal quenching data of the emission spectrum, Mikami et al.[23] have estimated the Eu_{5d}-CBM gap to be approximatively 0.6 and 0.2 eV for $Ba_3Si_6O_{12}N_2$:Eu and $Ba_3Si_6O_9N_4$:Eu, respectively.

DOI: 10.1021/acs.jpcc.5b12361
J. Phys. Chem. C 2016, 120, 4040−4047

To validate the Dorenbos' model, we build a global picture of the level positions for the absorption and emission in the two compounds, see Figure 2. Values mentioned in this figure come from different theoretical or experimental sources. First, we take accurate many-body G_0W_0 *ab initio* band gaps of 6.88 and 6.45 eV for the two host materials.[6] For the absorption, the 4f−5d gaps of 310 nm (4 eV) and 450 nm (2.75 eV) in $Ba_3Si_6O_{12}N_2$:Eu come from the peak and shoulder positions of the experimental absorption spectrum.[7] The equivalent 4f−5d gaps in $Ba_3Si_6O_9N_4$:Eu are located at 340 nm (3.65 eV) and 380 nm (3.26 eV). Similar considerations lead us to 5d−4f gaps of 535 nm (2.32 eV) and 485 nm (2.56 eV) for $Ba_3Si_6O_{12}N_2$:Eu and $Ba_3Si_6O_9N_4$:Eu, respectively. There is an additional blue shift of 0.06 eV at 300 K in the emission curve in the case of $Ba_3Si_6O_{12}N_2$:Eu.[7] Figure 2 is then confirmed and completed (in red) by the present first-principles results, as explained later.

Let us emphasize the meaning of the energy changes that are gathered in Figure 2. At variance with standard density-functional theory (DFT) band structures[26] or even GW quasi-particle band structures,[27] the levels inside the gap are not associated with the removal or addition of an electron but instead to neutral excitations. The Eu_{4f} level is occupied by seven electrons in the ground state (half-filled shell). The absorption of a photon leaves a hole in this Eu_{4f} shell and the electron that is transferred in the 5d lower levels or in the CBM feels the attractive potential of the hole, which is absent in traditional band structure methods. On the other hand, the band edges keep their usual significance: they weakly feel the localized 4f hole, since the corresponding electron (or hole) band edge states are delocalized.

3. THE GROUND STATE

3.1. Methodology and Numerical Parameters. The calculations were performed using the ABINIT software[28] with the projector augmented wave method (PAW),[29] and the Perdew−Burke−Ernzerhof (PBE) parametrization of the generalized gradient approximation (GGA)[30] for exchange-correlation functional.[26]

We have generated PAW atomic data sets for Ba and Eu taking the $4d^{10}5s^25p^66s^2$ (20 electrons) and the $4d^{10}5s^25p^64f^76s^2$ (27 electrons) orbitals as valence states and we have frozen the states below in the core. A computationally more affordable version of the Eu pseudopotential was generated using the same cutoff radii but placing the $4f^7$ and $4d^{10}$ electrons frozen in the core of the pseudopotential (10 electrons). The other PAW pseudopotentials (Si, O, N) were taken from the ABINIT Web site.[31]

To account for the strong correlation of these states, that DFT-PBE is unable to reproduce, we used the fully rotationally invariant formulation of GGA+U (U = 7.5 eV and J = 0.6 eV) with the double counting term in the fully localized limit.[32,33] The GGA+U correctly places the Eu_{4f} levels inside the bandgap of the host material in the ground state, as expected from experiment. We have checked that significant deviation (±1 eV) around the initial U value had no noticeable effect on all the other bands.

A plane-wave cutoff energy of 30 Ha and 35 Ha was used to describe the wave functions for the two supercells $Eu_1Ba_8Si_{18}O_{36}N_6$ and $Eu_1Ba_8Si_{18}O_{27}N_{12}$, respectively (see next subsection.). The integration over the Brillouin zone was performed on a 2 × 2 × 2 Monkhorst−Pack mesh,[34] half-shifted along the three Cartesian direction of the rhombohedral supercell.

3.2. Atomic Geometry in the Ground State. The crystal structure of the two hosts, where the Ba atom has two inequivalent positions in $Ba_3Si_6O_{12}N_2$ and three in $Ba_3Si_6O_9N_4$, is presented in ref 6, and their crystalline environment is represented in Figure 3. The five cases will be investigated here.

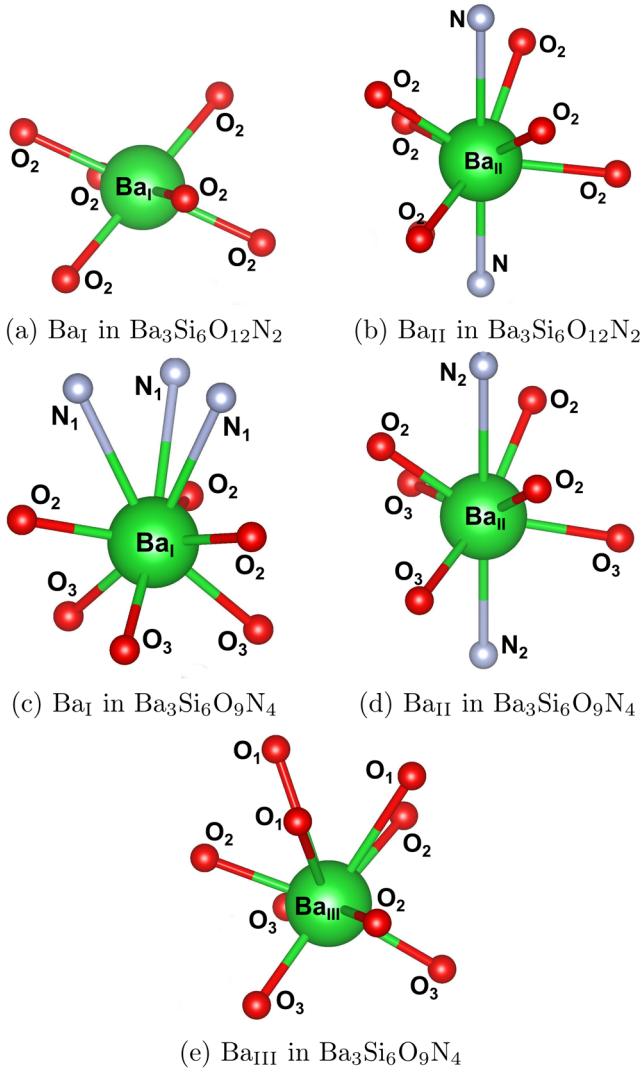

Figure 3. Crystalline environment of the two inequivalent Barium sites in $Ba_3Si_6O_{12}N_2$ are shown in parts (a) and (b). The three inequivalent one in $Ba_3Si_6O_9N_4$ are shown in parts (c), (d), and (e). Bond lengths are reported in Table 1.

By replacing one Ba atom of the primitive cell by an Eu one, the doping concentration is 33%, much higher than the 2−10% experimental doping.[17] Therefore, we relied on doped supercells that are three times larger than the primitive ones, $Eu_1Ba_8Si_{18}O_{36}N_6$ and $Eu_1Ba_8Si_{18}O_{27}N_{12}$, leading to an Eu doping concentration of 11%.

The primitive cell of $Ba_3Si_6O_{12}N_2$ has a $P\bar{3}$ (trigonal,147) space group whereas $Ba_3Si_6O_9N_4$ has a $P3$ (trigonal,143) space group. By replacing one Ba atom of the supercell by an Eu one, we maintain a $R\bar{3}$ (rhombohedral,148) space group for the first Eu substitution in $Ba_3Si_6O_{12}N_2$, but lower the symmetry for the second one, with a $R3$ (rhombohedral,146) space group. For $Ba_3Si_6O_9N_4$, the three substitution cases maintain the $R\bar{3}$ (rhombohedral,148) space group.

DOI: 10.1021/acs.jpcc.5b12361
J. Phys. Chem. C 2016, 120, 4040−4047

The structural relaxation with the 10 electrons pseudopotential for Eu leads to a lattice parameter of 10.001 Å with a rhombohedral angle of 81.889° for the Eu_I substitution and a lattice parameter of 9.992 Å with a rhombohedral angle of 82.456° for the Eu_{II} substitution of $Ba_9Si_{18}O_{36}N_6$. The three substitutions Eu_I, Eu_{II} and Eu_{III} in $Ba_9Si_{18}O_{27}N_{12}$ have lattice parameters that are calculated to be 9.998 Å, 9.985 and 9.990 Å with rhombohedral angles of 78.371°, 78.680°, and 78.339°. The bonds lengths are compared with respect to the undoped case in Table 1. The Eu-doped structures are contracted with respect to the undoped compounds investigated previously in ref 6. This seems reasonable given that the experimental atomic radius of Eu is 1.31 Å, smaller than the 1.49 Å atomic radius of Ba[35] (both of them taken in their VI coordination state). As expected, we observed a rather strong contraction of the bonds around the substituted Eu atoms with up to 10% of Eu−O bond contraction in the case of $Eu_{II}Ba_8Si_{18}O_{27}N_{12}$. The overall cell volume is contracted by 1.5% and 1.9% with respect to the undoped case for the Eu_I and Eu_{II} substitutions in $Ba_9Si_{18}O_{36}N_6$. An equivalent contraction of 1.5%, 1.9%, and 1.8% happens for Eu_I, Eu_{II}, and Eu_{III} in $Ba_9Si_{18}O_{27}N_{12}$, respectively. See Table 1 for more details.

Table 1. Selected Bond Lengths [in Å] of $Ba_3Si_6O_{12}N_2$ and $Ba_3Si_6O_9N_4$ Compounds, either Undoped or Doped with Europium[a]

	$Ba_3Si_6O_{12}N_2$				
		ground state		excited state	
	undoped[b]	Eu	diff %	Eu	diff %
X_I−O_2 (6×)	2.760	2.532	−8.3	2.388	−13.5
X_{II}−O_2 (3×)	2.959	2.869	−3.0	2.798	−5.4
X_{II}−O_2 (3×)	2.812	2.528	−10.1	2.352	−16.4
X_{II}−N (1×)	3.054	2.878	−5.8	2.763	−9.5
X_{II}−N (1×)	3.499	3.464	−1.0	3.578	2.3
		$Ba_3Si_6O_9N_4$			
X_I−O_2 (3×)	2.714	2.561	−5.6	2.414	−11.0
X_I−O_3 (3×)	2.823	2.582	−8.5	2.489	−11.8
X_I−N_1 (3×)	3.498	3.729	6.6	3.768	7.7
X_{II}−O_2 (3×)	2.703	2.437	−9.8	2.343	−13.3
X_{II}−O_3 (3×)	2.860	2.758	−3.6	2.629	−8.1
X_{II}−N_2 (1×)	3.284	3.183	−3.1	3.059	−6.8
X_{II}−N_2 (1×)	3.579	3.469	−3.1	3.593	0.4
X_{III}−O_2 (3×)	2.730	2.535	−7.2	2.421	−11.3
X_{III}−O_3 (3×)	2.731	2.553	−6.5	2.450	−10.3
X_{III}−O_1 (3×)	3.375	3.579	6.0	3.388	0.4

Shannon Crystal Radii[c]		
ion	coordination	crystal radius
Ba^{2+}	VI/VII	1.49/1.52
Eu^{2+}	VI/VII	1.31/1.34
Eu^{3+}	VI/VII	1.08/1.15
O^{2-}	VI	1.26
N^{3-}	IV	1.32
Si^{4+}	IV	0.40

[a]X denotes either Ba (in the undoped case) or Eu (in the doped cases). [b]See ref 6. [c]See ref 35.

The total energy of the Eu_I and Eu_{II} substitution in $Ba_9Si_{18}O_{36}N_6$ is −2408.536901 Ha and −2408.531555 Ha, respectively. This means that the first substitution site will be favored by 0.048 eV (1.1 kcal/mol) per unit formula. This is slightly above the 1 kcal/mol chemical accuracy. The total energy of the Eu_I, Eu_{II}, and Eu_{III} substitution in $Ba_9Si_{18}O_{27}N_{12}$ is −2323.139501 Ha, −2323.138339 Ha, and −2323.141829 Ha, respectively. In this case, the most stable substitution is Eu_{III}, 0.031 eV (0.7 kcal/mol) per unit formula lower that the least stable one (Eu_{II}). The high firing temperature (≈1200−1600 °C) at which the compounds are produced corresponds to a thermal energy of about 0.13 eV. For this reason, all substitution positions are expected to occur, and we will therefore study the excited state properties of all the five cases.

4. THE EXCITED STATE

Using the above-mentioned GGA+U at the relaxed ground-state atomic positions lead to Eu_{5d} bands that are not localized inside the bandgap of the host material, in contradiction to both the 5d−4f crossing decay model and the Dorenbos autoionization model. For $Ba_3Si_6O_{12}N_2$:Eu, this had already been noticed in ref 36. To get the correct picture where the 5d levels are correctly located inside the band gap of the host materials, we need to rely on another scheme.

4.1. Depletion of the 4f Shell. As already mentioned, the presence of Eu_{5d} states inside the band gap in Figure 2 is due to the hole left by the Eu_{4f} to Eu_{5d} transition, creating an attractive center for the Eu_{5d} electron. The Eu_{5d} electron and the Eu_{4f} hole are strongly bound to each other and their description would require a cumbersome treatment at the BSE level. To make the problem tractable, we use two simpler mean-field approaches that allow us to describe the Coulomb effect of the hole while the Eu_{5d} state is occupied. In the first one, the pseudopotential core-hole approach (see for example ref 37), a $4f^6$ shell is frozen in the pseudopotential, instead of the ground state $4f^7$ shell. We have therefore created a core-hole pseudopotential by removal of an electron from the 4f state of the 27 electrons pseudopotential presented earlier. In the second approach, the Eu_{4f} hole is treated explicitly in the valence manifold through forced occupation numbers of the Eu_{4f} orbitals (equal occupation numbers). This approach is called "constrained DFT" (CDFT) and has been applied successfully to a wide range of materials,[38−42] including rare-earth doped solid-state compounds, by Canning and co-workers, to study the luminescence in Ce-doped[43,44] and Eu-doped[45] inorganic scintillators. In both approaches, the Coulomb interaction is correctly included between the Eu core and the explicitly treated Eu_{5d} electron, as well as between the electrons and the other nuclei, allowing to include the most relevant physics in the computation of the forces, and thus yielding reasonable atomic geometries.

4.2. Atomic Geometry in the Excited State. After the absorption, the excited electron will impact its surrounding and atoms will move as the result of electrostatic interaction. The electron will then re-emit a photon and go back to the ground state. If the electron stays a short amount of time in its excited state, it will not affect the macroscopic state of the crystal (unlike the local geometry) so that the lattice parameters of the crystal will not change significantly. Therefore, we have only considered atomic relaxation at the fixed lattice parameters of the ground state.

The bonds lengths between the Europium atom and the neighboring atoms after relaxation in the excited state, using the pseudopotential core-hole approach described in the previous subsection, to relax the geometries from first principles are given in Table 1. The contraction of the O cage around the Eu atom can be extremely important for some bonds, e.g. up to 16% contraction of the Eu−O bond length with respect to the

DOI: 10.1021/acs.jpcc.5b12361
J. Phys. Chem. C 2016, 120, 4040−4047

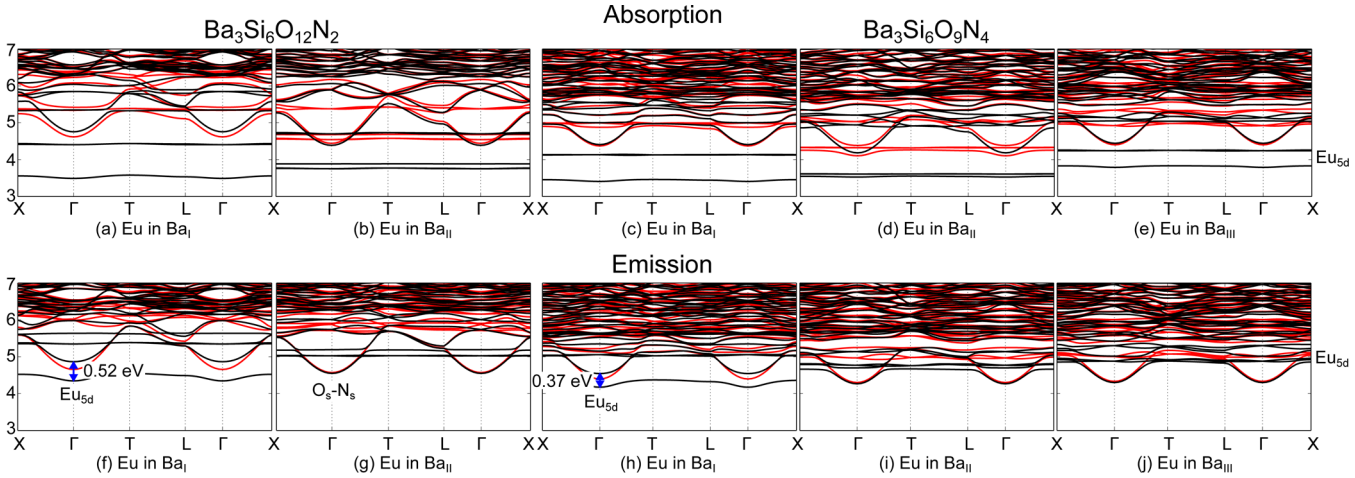

Figure 4. Spin-polarized (up in black and down in red) bandstructures corresponding to the absorption (ground-state relaxed atomic positions) and emission (excited-state relaxed positions), in a rhombohedral supercell. One of the nine Ba atoms is replaced by an Eu one at the I, II, or III inequivalent Ba positions, leading to an effective Eu doping of 11%. The zero energy is positioned at the top of the valence band of the host materials and is not shown here. For the emission, cases (f) and (h) are the luminescent ones whereas the three others are not due to the fact that their Eu_{5d} band is localized above the CBM of the host material.

undoped case. This level of additional contraction is well in line with the change of cation radii associated with the change of oxidation state for the Eu atom that we describe.[35] The atomic relaxations of the excited states are performed with the core-hole pseudopotential to capture the electron−hole interaction. For these relaxations, the Coulomb interaction between the neighboring atoms and the Eu_{5d} electron must be accounted for, so that the occupation of the Eu_{5d} state is enforced.

5. IONIZATION FROM THE 5D STATE TO THE CONDUCTION BAND

5.1. Self-Interaction in the Excited State: the Depleted-Shifted 4f Approach. However, producing an electronic bandstructure at these excited atomic geometries with either the core-hole or the CDFT approach prove to be quite deceiving, as they include a nonphysical self-interaction of the excited electron in the Eu_{5d} and they poorly describe many-body effects in both Eu_{5d} and the CBM. The self-interaction overscreens the electronic properties and push the Eu_{5d} too high in energy, comparatively to the CBM.

In order to describe the electronic properties properly, a self-interaction free method has to be used. We found out that even the simple Kohn−Sham band structure obtained with the depleted Eu_{4f} shell charge density, but *without occupying the Eu_{5d} orbitals, nor the conduction band minimum* has no (or little) self-interaction bias between these states. This is further validated in section 6.

Moreover, the use of GGA+U is not enough to localize the Eu_{4f} states inside the bandgap when an electron is removed. An additional atomic potential energy shift of 0.3 Ha for $Ba_3Si_6O_{12}N_2$ and 0.28 Ha for $Ba_3Si_6O_9N_4$ has to be applied on the Eu_{4f} states in order to reproduce the known experimental data shown in Figure 2. Since this additional atomic potential is applied in the same way for the two sets, we can still discuss their relative difference. We propose to name this hybrid method "depleted-shifted 4f approach" as we remove one electron and apply an additional atomic potential energy to those 4f states. An homogeneous negative background is also added to preserve charge neutrality.

5.2. The 5d and Conduction Band Levels in the Case of Neutral Excitations. The 5d and conduction band levels, obtained with a mean-field 4f hole in the depleted-shifted 4f approach, were computed for the rhombohedral Eu-doped supercells with different geometries. The results with ground-state atomic positions (absorption) are shown in parts (a)−(e) of Figures 4, while those associated with the emission process, computed at the relaxed atomic positions, are presented in parts (f)−(j) of Figure 4. The differences between ground-state and excited-state geometries are large, and crucial to correctly describe the emission process: in all five cases, the absorption geometry leads to two (or three) Eu_{5d} levels below the CBM (dispersive band), while this only happens in two cases for the relaxed geometry with only one Eu_{5d} band.

From the analysis of the emission in Figure 4, we conclude that the two Eu_I substitutions in $Ba_9Si_{18}O_{36}N_6$ and $Ba_9Si_{18}O_{27}N_{12}$ are the only luminescent centers due to the position of their Eu_{5d} band below the CBM, as expected from the small fwhm. We found out that the two Eu_{5d}-CBM gaps are 0.52 and 0.37 eV for $Eu_IBa_8Si_{18}O_{36}N_6$ and $Eu_IBa_8Si_{18}O_{27}N_{12}$, respectively.

To strengthen our analysis, we notice that the lowest conduction bands of the three nonluminescent centers, parts (g), (i), and (j) of Figure 4 are spin degenerate because the delocalized states are far from the Eu atom and therefore do not react to its magnetic moment. We have also made an analysis of the change of 4f state energy with respect to the 5d-CBM gap, for intermediate geometries. We observe that the 5d-CBM gap closes well before the 4f energy comes close to the 5d energy, supporting the Dorenbos model.

6. ADDITIONAL TESTS AND DISCUSSION

6.1. Validation of the Depleted-Shifted 4f Approach. In order to validate our hybrid method, we have performed tests, for the primitive cell only, based on the BSE and the GW methodology. In particular, we note that the BSE builds an effective Hamiltonian that takes into account two Feynman diagrams: the direct (attractive Coulomb interaction) diagram and the exchange diagram.[22] The attractive screened Coulomb interaction obtained from the BSE is accounted for to a large

DOI: 10.1021/acs.jpcc.5b12361
J. Phys. Chem. C 2016, 120, 4040−4047

extend in the core-hole and depleted-shifted 4f techniques because the change of the electronic potential resulting from the hole in the pseudopotential is computed self-consistently within DFT (screened electron−hole interaction) and because all 4f states are strongly localized. In contrast, the exchange term V_{xc} within DFT is only a one-point function and therefore does not have the adequate form to reproduce the four-point kernel function of the BSE. To evaluate the crudeness of the mean-field approach, we have computed in a restricted space of valence and conduction states, the Bethe−Salpeter exchange term for the $Ba_3Si_6O_{12}N_2$:Eu compound. We have obtained that the effect of the exchange could be as large as 0.25 eV in high-lying excitonic states, but the lowest transitions were nearly unaffected (0.02 eV). Also, we have performed GW calculations on the doped primitive cell, with the core-hole Eu pseudopotential. The relative changes, between the Eu_{5d} and the conduction band minimum, compared to the Kohn−Sham eigenenergies, were much smaller than the GW corrections for the valence to conduction band gap of the host materials. The latter corrections were on the order of 2.1−2.2 eV for the host materials,[6] while the GW correction to the Eu_{5d} to CBM gap were only on the order of 0.2−0.3 eV.

6.2. The Spin−Orbit Coupling. For the sake of completeness, we have investigated the effect of spin−orbit coupling in such BSON compounds using the Vienna *ab initio* software package (VASP).[46] The spin−orbit coupling lifts the Eu_{4f} degeneracies and the levels become more dispersive. The inclusion of spin−orbit coupling leads to no noticeable difference on all the other bands except the Eu_{4f}. The set of Eu_{4f} bands has a spread of 0.24 eV when only spin-polarization is included and broaden to 0.56 eV when spin−orbit coupling is included.

6.3. Probability of Substitution Site Occupation. The bond valence model developed by Brown and Altermatt provides a quantitative description of inorganic bonding.[47,48] In this model, all atoms are considered to be cations or anions depending on their oxidation state and all pairs of atoms i and j are considered to be bonds with varying strength s_{ij}. The bond strength is computed following the relation

$$s_{ij} = e^{(r_{0,ij} - r_{ij})/B} \quad (1)$$

with r_{ij} the distance between the two atoms, $r_{0,ij}$ an empirical parameter tabulated for each bond type, and B an empirical constant whose value is kept constant to 0.37 for all bonds.[47] In the case of Ba−O bonds $r_{0,ij}$ = 2.285 (averaged on 254 materials from the ICSD database)[47] and $r_{0,ij}$ = 2.47 for the Ba−N bonds.[49]

The sum of the bond strengths around an ion i is called the bond valence sum (BVS)

$$V_i = \sum_j s_{ij} \quad (2)$$

and should approximate the charge of the ion.

Using the bond distances given in Table 1, the BVS for the Ba atom at the inequivalent crystallographic positions in the undoped compounds can be computed. We obtain a BVS of 1.938 and 1.838 for Ba_I and Ba_{II} in $Ba_3Si_6O_{12}N_2$, respectively. The BVS is calculated to be 1.944, 1.805, and 2.052 for Ba_I, Ba_{II}, and Ba_{III} in $Ba_3Si_6O_9N_4$, respectively.

Upon doping, the smaller Eu^{2+} atom is expected to substitute mainly the site with the highest BVS (first site in $Ba_3Si_6O_{12}N_2$ and third site in $Ba_3Si_6O_9N_4$). This model further confirm our finding based on *ab initio* total energy stability presented at the end of section 3.2 and leads to the exact same conclusion.

However, experimental evidence[10,12,18,50] suggest that the substituted Eu^{2+} atoms are randomly distributed across all substitution sites (may it be with uneven probability density). As already mentioned in Section 3.2, we attribute such random distribution of the Eu atoms substitution to the high firing temperature and the fact that Ba^{2+} atoms form layers in BSON crystals.

6.4. Temperature Dependence of CBM of the Undoped Hosts. Finally, we also studied the effect of temperature on the CBM of the two BSON host materials, using the static Allen−Heine−Cardona (AHC) theory.[51−56]

Because of the constraints in the current implementation of the AHC theory in ABINIT, we had to use norm-conserving pseudopotentials. The valence electrons of Ba, Si, O, and N, treated explicitly in the *ab initio* calculations, are the $6s^2$, $3s^23p^2$, $2s^22p^4$, and $2s^22p^3$ orbitals, respectively. Noticeably, we decided not to use the semicore version of the Ba pseudopotential to decrease the computational load. These pseudopotentials reproduce the experimental or PAW lattice parameters sufficiently well as detailed now. The DFT structural relaxation of both compounds leads to hexagonal lattice constants of a = 7.616 Å and c = 6.684 Å for $Ba_3Si_6O_{12}N_2$ and a = 7.353 Å and c = 6.995 Å for $Ba_3Si_6O_9N_4$. With respect to the relaxed lattice parameter obtained using PAW and semicore states for Ba presented in ref6., the a parameter is 0.1% and the c parameter is 2% larger for $Ba_3Si_6O_{12}N_2$. In the case of $Ba_3Si_6O_9N_4$, the a lattice parameter is 0.4% larger and the c parameter is 1.9% larger. For the AHC calculations, the phonon **q**-point grid integration was computed on a 4 × 4 × 4 **q**-point grid with a 100 meV smearing and lead to a similar renormalization of −0.17 eV for both compounds at 300 K. The slopes at high temperature are −0.391 and −0.377 meV/K for $Ba_3Si_6O_{12}N_2$ and $Ba_3Si_6O_9N_4$, respectively. The full temperature-dependence is given on Figure 5.

At present, AHC calculations for the doped materials are out of reach computationally. Still, we do not expect large relative

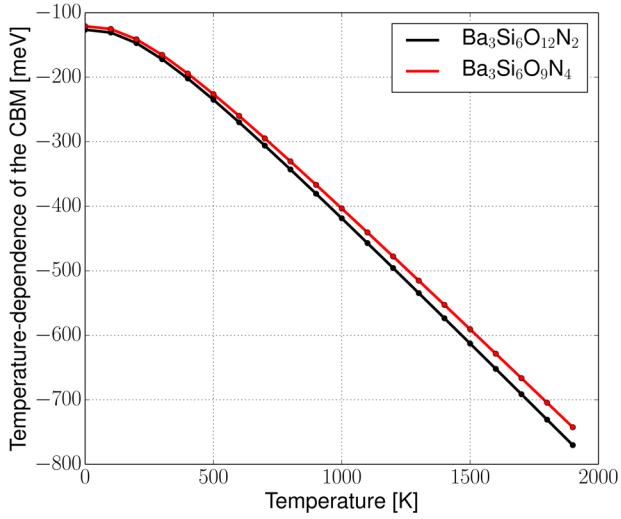

Figure 5. Temperature-dependence of the conduction band minimum (Γ-point) for the two undoped BSON compounds within the static AHC theory integrated on a 4 × 4 × 4 **q**-point grid with a 100 meV smearing. The slopes at high temperature are −0.391 and −0.377 meV/K for $Ba_3Si_6O_{12}N_2$ and $Ba_3Si_6O_9N_4$, respectively.

DOI: 10.1021/acs.jpcc.5b12361
J. Phys. Chem. C 2016, 120, 4040−4047

differences between the two materials, and in any case much smaller than the −0.17 eV renormalization of the CBM.

7. CONCLUSION

All of the above-mentioned results allow us to complete our schematic drawing of Figure 2, yielding a global picture on which theory and experiment agree. From Figure 4, we also identify the only active luminescent center in both $Ba_3Si_6O_{12}N_2$ and $Ba_3Si_6O_9N_4$. The three other nonequivalent centers have their Eu_{5d} states completely above the CBM level of the host material therefore leading to nonradiative emissions. This confirms the experimental results that show narrow and well resolved emission peaks for the two BSON compounds as well as experimentally verified nonradiative sites in those materials.[57] Figure 4 has been obtained through the depleted-shifted 4f scheme, whose validity was checked by comparing it to the Bethe-Salpeter theory in a simplified case. As seen in Figure 4, the relaxation of the Eu doped excited state is of crucial importance as there are major changes in the electronic bandstructure before and after Stokes shifts. We confirm the Dorenbos autoionization model: the Eu_{5d}-CBM gap is 0.09 eV larger in $Ba_3Si_6O_{12}N_2$:Eu than in $Ba_3Si_6O_9N_4$:Eu. This energy difference is enough to show significant thermal quenching behavior differences.[25] The techniques that we have used, for the ground state, for the excited state, and finally, for the study of the gap with the conduction band, should be widely applicable for realistic models of phosphors at a much lower computational cost than the much more expensive BSE technique. We hope that our work will raise experimental interest into the extensive characterization of each photoluminescent site in both compounds.

AUTHOR INFORMATION

Corresponding Author

*(S.P.) E-mail: samuel.pon@gmail.com. Telephone: +44 7480933330.

Notes

The authors declare no competing financial interest.

ACKNOWLEDGMENTS

We acknowledge discussions with B. Bertrand and D. Waroquiers, and thank J.-M. Beuken for computational help. This work has been supported by the Fonds de la Recherche Scientifique (FRS-FNRS Belgium) through a FRIA fellowship (S.P.) and the PdR Grant No. T.0238.13 - AIXPHO. Computational ressources have been provided by the supercomputing facilities of the Université catholique de Louvain (CISM/UCL) and the Consortium des Equipements de Calcul Intensif en Fédération Wallonie Bruxelles (CECI) funded by the FRS-FNRS under Grant No. 2.5020.11.

REFERENCES

(1) Sato, Y.; Kato, H.; Kobayashi, M.; Masaki, T.; Yoon, D.-H.; Kakihana, M. Tailoring of Deep-Red Luminescence in Ca_2SiO_4:Eu^{2+}. *Angew. Chem., Int. Ed.* **2014**, *53*, 7756−7759.

(2) Bardsley, N.; Bland, S.; Hansen, M.; Pattison, L.; Pattison, M.; Stober, K.; Yamada, M. *Solid-State Lighting R&D Plan, a Report from Solid-State Lighting Program* **2015**, DOI: 10.2172/1220487.

(3) Henry, B. R.; Kasha, M. Radiationless Molecular Electronic Transitions. *Annu. Rev. Phys. Chem.* **1968**, *19*, 161−192.

(4) Englman, R.; Barnett, B. Quantitative Theory of Luminescent Centres in a Configurational Diagram Model: I. Description of the Method. *J. Lumin.* **1970**, *3*, 37−54.

(5) Khan, T.; Bodrogi, P.; Vinh, Q.; Winkler, H. In *LED Lighting: Technology and Perception*; Khan, T., Bodrogi, P., Vinh, Q., Winkler, H., Eds.; Wiley: Weinheim, Germany, 2015.

(6) Bertrand, B.; Poncé, S.; Waroquiers, D.; Stankovski, M.; Giantomassi, M.; Mikami, M.; Gonze, X. Quasiparticle Electronic Structure of Barium-Silicon Oxynitrides for White-LED Application. *Phys. Rev. B: Condens. Matter Mater. Phys.* **2013**, *88*, 075136.

(7) Uheda, K.; Shimooka, S.; Mikami, M.; Imura, H.; Kijima, N. Synthesis and Characterization of New Green Phosphor for White LED. *Proc. IDW '07* **2007**, 899−902.

(8) Mikami, M.; Shimooka, S.; Uheda, K.; Imura, H.; Kijima, N. New Green Phosphor $Ba_3Si_6O_{12}N_2$:Eu for White LED: Crystal Structure and Optical Properties. *Key Eng. Mater.* **2009**, *403*, 11−14.

(9) Zhang, R.; Numata, M.; Maeda, T.; Akazawa, Y.; Murai, K.-I.; Moriga, T. Preparation And Luminescence Properties Of Eu^{2+}-Activated Ba-Si_x-O-N Phosphors. *Int. J. Mod. Phys. B* **2010**, *24*, 3221−3225.

(10) Braun, C.; Seibald, M.; Börger, S.; Oeckler, O.; Boyko, T.; Moewes, A.; Miehe, G.; Tücks, A.; Schnick, W. Material Properties and Structural Characterization of $M_3Si_6O_{12}N_2$:Eu^{2+} (M = Ba, Sr)- A Comprehensive Study on a Promising Green Phosphor for pc-LEDs. *Chem. - Eur. J.* **2010**, *16*, 9646−9657.

(11) Tang, J.; Chen, J.; Hao, L.; Xu, X.; Xie, W.; Li, Q. Green Eu^{2+}-Doped $Ba_3Si_6O_{12}N_2$ Phosphor for White Light-Emitting Diodes: Synthesis, Characterization and Theoretical Simulation. *J. Lumin.* **2011**, *131*, 1101−1106.

(12) Porob, D. G.; Kishore Manepallib, S.; Kumarb, N. P.; Setlur, A. Synthesis and Luminescence Properties of Green Oxynitride Phosphor. *ECS Trans.* **2011**, *33*, 101−107.

(13) Song, Y. H.; Choi, T. Y.; Senthil, K.; Masaki, T.; Yoon, D. H. Photoluminescence Properties of Green-Emitting Eu^{2+}-Activated $Ba_3Si_6O_{12}N_2$ Oxynitride Phosphor for White LED Applications. *Mater. Lett.* **2011**, *65*, 3399−3401.

(14) Kang, E.-H.; Choi, S.-W.; Hong, S.-H. Synthesis of $Ba_3Si_6O_{12}N_2$:Eu^{2+} Green Phosphors Using Ba_3SiO_5:Eu^{2+} Precursor and Their Luminescent Properties. *ECS J. Solid State Sci. Technol.* **2012**, *1*, R11−R14.

(15) Chen, G.; Zhuang, W.; Hu, Y.; Liu, Y.; Liu, R.; He, H. Luminescence Properties of Eu^{2+}-Doped $Ba_3Si_6O_{12}N_2$ Green Phosphor: Concentration Quenching and Thermal Stability. *J. Rare Earths* **2013**, *31*, 113−118.

(16) Chen, G.; Zhuang, W.; Liu, R.; Liu, Y.; Hu, Y.; He, H. Photoluminescent Properties of Tunable Green-Emitting Oxynitride $(Ba_{3-x}Sr_x)Si_6O_{12}N_2$:$Eu^{2+}$ Phosphor and its Application in White LEDs. *J. Rare Earths* **2013**, *31*, 944−949.

(17) Li, W.; Xie, R.-J.; Zhou, T.; Liu, L.; Zhu, Y. Synthesis of the Phase Pure $Ba_3Si_6O_{12}N_2$:Eu^{2+} Green Phosphor and its Application in High Color Rendition White LEDs. *Dalton Trans.* **2014**, *43*, 6132−6138.

(18) Stadler, F.; Schnick, W. The New Layer-Silicates $Ba_3Si_6O_9N_4$ and $Eu_3Si_6O_9N_4$. *Z. Anorg. Allg. Chem.* **2006**, *632*, 949−954.

(19) Song, S.-H.; Chung, E.-J.; Song, Y.-H.; Jung, M.-K.; Yoon, D.-H. Photoluminescence Properties of Eu^{2+}-Doped $Ba_3Si_6O_9N_4$ Phosphors Synthesized by a Gas Reduction Nitridation Method for White Light Emitting Diodes. *Phys. Scr.* **2013**, *157*, 014052.

(20) Li, C.; Chen, H.; Hua, Y.; Yu, L.; Jiang, Q.; Deng, D.; Zhao, S.; Ma, H.; Xu, S. Enhanced Luminescence of $Ba_3Si_6O_9N_4$:Eu^{2+} Phosphors by Codoping with Ce^{3+}, Mn^{2+}, and Dy^{3+} Ions. *J. Lumin.* **2013**, *143*, 459−462.

(21) Kim, H.-G.; Kang, E.-H.; Kim, B.-H.; Hong, S.-H. Preparation and Luminescence Properties $Ba_3Si_6O_9N_4$:Eu^{2+} of Phosphor. *Opt. Mater.* **2013**, *35*, 1279−1282.

(22) Onida, G.; Reining, L.; Rubio, A. Electronic Excitations: Density-Functional versus Many-Body Green's-Function Approaches. *Rev. Mod. Phys.* **2002**, *74*, 601−659.

(23) Mikami, M.; Kijima, N.; Bertrand, B.; Stankovski, M.; Gonze, X. Theoretical Approach for White-LED Phosphors: from Crystal Structures to Optical Properties. *IOP Conf. Ser.: Mater. Sci. Eng.* **2011**, *18*, 102001.

DOI: 10.1021/acs.jpcc.5b12361
J. Phys. Chem. C 2016, 120, 4040−4047

(24) Mikami, M. Response Function Calculations of $Ba_3Si_6O_{12}N_2$ and $Ba_3Si_6O_9N_4$ for the Understanding of the Optical Properties of the Eu-doped Phosphors. *Opt. Mater.* **2013**, *35*, 1958−1961.
(25) Dorenbos, P. Thermal Quenching of Eu^{2+} 5d-4f Luminescence in Inorganic Compounds. *J. Phys.: Condens. Matter* **2005**, *17*, 8103−8111.
(26) Martin, R. M. *Electronic Structure. Basic Theory and Practical Methods*; Cambridge University Press: 2004; p 650.
(27) Aulbur, W. G.; Jönsson, L.; Wilkins, J. W. In *Quasiparticle Calculations in Solids*; Ehrenreich, H., Spaepen, F., Eds.; Solid State Physics 54; Academic Press: 1999; pp 1−218.
(28) Gonze, X.; Amadon, B.; Anglade, P.-M.; Beuken, J.-M.; Bottin, F.; Boulanger, P.; Bruneval, F.; Caliste, D.; Caracas, R.; Côté, M.; et al. ABINIT: First-Principles Approach to Material and Nanosystem Properties. *Comput. Phys. Commun.* **2009**, *180*, 2582−2615.
(29) Blöchl, P. E. Projector Augmented-Wave Method. *Phys. Rev. B: Condens. Matter Mater. Phys.* **1994**, *50*, 17953.
(30) Perdew, J. P.; Burke, K.; Ernzerhof, M. Generalized Gradient Approximation Made Simple. *Phys. Rev. Lett.* **1996**, *77*, 3865−3868.
(31) http://www.abinit.org/downloads/PAW2.
(32) Liechtenstein, A. I.; Anisimov, V. I.; Zaanen, J. Density-Functional Theory and Strong Interactions: Orbital Ordering in Mott-Hubbard Insulators. *Phys. Rev. B: Condens. Matter Mater. Phys.* **1995**, *52*, R5467−R5470.
(33) Amadon, B.; Jollet, F.; Torrent, M. α and β Cerium: LDA+U Calculations of Ground-State Parameters. *Phys. Rev. B: Condens. Matter Mater. Phys.* **2008**, *77*, 155104.
(34) Monkhorst, H. J.; Pack, J. D. Special Points for Brillouin-Zone Integrations. *Phys. Rev. B* **1976**, *13*, 5188−5192.
(35) Shannon, R. D. Revised Effective Ionic Radii and Systematic Studies of Interatomic Distances in Halides and Chalcogenides. *Acta Crystallogr., Sect. A: Cryst. Phys., Diffr., Theor. Gen. Crystallogr.* **1976**, *32*, 751−767.
(36) Tang, J.-Y.; Gao, J.-K.; Chen, J.-H.; Hao, L.-Y.; Xu, X.; Lee, M.-H. Contribution of Cations to the Photoluminescence Properties of Eu-Doped Barium Oxonitridosilicates Phosphors. *Comput. Mater. Sci.* **2013**, *79*, 478−484.
(37) Pehlke, E.; Scheffler, M. Evidence for Site-Sensitive Screening of Core Holes at the Si and Ge (001) Surface. *Phys. Rev. Lett.* **1993**, *71*, 2338−2341.
(38) Dederichs, P.; Blügel, S.; Zeller, R.; Akai, H. Ground States of Constrained Systems: Application to Cerium Impurities. *Phys. Rev. Lett.* **1984**, *53*, 2512.
(39) Marsman, M.; Andriessen, J.; van Eijk, C. W. E. Structure, Optical Absorption, and Luminescence Energy Calculations of Ce^{3+} Defects in $LiBaF_3$. *Phys. Rev. B: Condens. Matter Mater. Phys.* **2000**, *61*, 16477.
(40) Wu, Q.; Van Voorhis, T. Direct Optimization Method to Study Constrained Systems within Density-Functional Theory. *Phys. Rev. A: At., Mol., Opt. Phys.* **2005**, *72*, 024502.
(41) Wu, Q.; Van Voorhis, T. Direct Calculation of Electron Transfer Parameters Through Constrained Density Functional Theory. *J. Phys. Chem. A* **2006**, *110*, 9212−9218.
(42) Kaduk, B.; Kowalczyk, T.; Van Voorhis, T. Constrained Density Functional Theory. *Chem. Rev.* **2012**, *112*, 321−370.
(43) Canning, A.; Chaudhry, A.; Boutchko, R.; Grønbech-Jensen, N. First-Principles Study of Luminescence in Ce-doped Inorganic Scintillators. *Phys. Rev. B: Condens. Matter Mater. Phys.* **2011**, *83*, 125115.
(44) Chaudhry, A.; Canning, A.; Boutchko, R.; Weber, M. J.; Grønbech-Jensen, N.; Derenzo, S. E. First-Principles Studies of Ce-Doped $RE_2M_2O_7$ (RE = Y, La; M = Ti, Zr, Hf): A Class of Nonscintillators. *J. Appl. Phys.* **2011**, *109*, 083708.
(45) Chaudhry, A.; Boutchko, R.; Chourou, S.; Zhang, G.; Grønbech-Jensen, N.; Canning, A. First-Principles Study of Luminescence in Eu-Doped Inorganic Scintillators. *Phys. Rev. B: Condens. Matter Mater. Phys.* **2014**, *89*, 155105.
(46) Kresse, G.; Furthmüller, J. Efficiency of Ab-Initio Total Energy Calculations for Metals and Semiconductors using a Plane-Wave Basis Set. *Comput. Mater. Sci.* **1996**, *6*, 15−50.
(47) Brown, I. D.; Altermatt, D. Bond-Valence Parameters Obtained from a Systematic Analysis of the Inorganic Crystal Structure Database. *Acta Crystallogr., Sect. B: Struct. Sci.* **1985**, *41*, 244−247.
(48) Altermatt, D.; Brown, I. D. The Automatic Searching for Chemical Bonds in Inorganic Crystal Structures. *Acta Crystallogr., Sect. B: Struct. Sci.* **1985**, *41*, 240−244.
(49) Brese, N. E.; O'Keeffe, M. Bond-Valence Parameters for Solids. *Acta Crystallogr., Sect. B: Struct. Sci.* **1991**, *47*, 192−197.
(50) Ermakova, O.; Paszkowicz, W.; Kaminska, A.; Barzowska, J.; Szczodrowski, K.; Grinberg, M.; Minikayev, R.; Nowakowska, M.; Carlson, S.; Li, G. Equation of State for Eu-Doped SrSi2O2N2. *J. Chem. Phys.* **2014**, *141*, 014705.
(51) Poncé, S.; Antonius, G.; Boulanger, P.; Cannuccia, E.; Marini, A.; Côté, M.; Gonze, X. Verification of First-Principles Codes: Comparison of Total Energies, Phonon Frequencies, Electron-Phonon Coupling and Zero-Point Motion Correction to the Gap between ABINIT and QE/Yambo. *Comput. Mater. Sci.* **2014**, *83*, 341.
(52) Poncé, S.; Antonius, G.; Gillet, Y.; Boulanger, P.; Laflamme Janssen, J.; Marini, A.; Côté, M.; Gonze, X. Temperature Dependence of Electronic Eigenenergies in the Adiabatic Harmonic Approximation. *Phys. Rev. B: Condens. Matter Mater. Phys.* **2014**, *90*, 214304.
(53) Antonius, G.; Poncé, S.; Boulanger, P.; Côté, M.; Gonze, X. Many-Body Effects on the Zero-Point Renormalization of the Band Structure. *Phys. Rev. Lett.* **2014**, *112*, 215501.
(54) Marini, A.; Poncé, S.; Gonze, X. Many-body Perturbation Theory Approach to the Electron-Phonon Interaction with Density-Functional Theory as a Starting Point. *Phys. Rev. B: Condens. Matter Mater. Phys.* **2015**, *91*, 224310.
(55) Poncé, S.; Gillet, Y.; Laflamme Janssen, J.; Marini, A.; Verstraete, M.; Gonze, X. Temperature Dependence of the Electronic Structure of Semiconductors and Insulators. *J. Chem. Phys.* **2015**, *143*, 102813.
(56) Antonius, G.; Poncé, S.; Lantagne-Hurtubise, E.; Auclair, G.; Gonze, X.; Côté, M. Dynamical and Anharmonic Effects on the Electron-Phonon Coupling and the Zero-Point Renormalization of the Electronic Structure. *Phys. Rev. B: Condens. Matter Mater. Phys.* **2015**, *92*, 085137.
(57) Komuro, N.; Mikami, M.; Saines, P. J.; Akimoto, K.; Cheetham, A. K. Deep Red Emission in Eu^{2+}-Activated $Sr_4(PO_4)_2O$ Phosphors for Blue-Pumped White LEDs. *J. Mater. Chem. C* **2015**, *3*, 7356−7362.

DOI: 10.1021/acs.jpcc.5b12361
J. Phys. Chem. C 2016, 120, 4040−4047